International Journal of Multiphase Flow 35 (2009) 34–46

Contents lists available at ScienceDirect

International Journal of Multiphase Flow

journal homepage: www.elsevier.com/locate/ijmulflow

Flow regime independent, high resolution multi-field modelling of near-horizontal gas–liquid flows in pipelines

M. Bonizzi [a,*], P. Andreussi [a,b], S. Banerjee [c]

[a] TEA Sistemi Spa, Viale della Liberta' 53. San Donato M.se (MI), Italy
[b] University of Pisa, Pisa, Italy
[c] Department of Chemical Engineering, City College, New York, USA

ARTICLE INFO

Article history:
Received 15 May 2008
Received in revised form 4 September 2008
Accepted 7 September 2008
Available online 21 September 2008

ABSTRACT

For fully-developed two-phase flows, maps that correlate experimental and semi-empirical expressions for flow regimes are widely used. For calculations of the various important two-phase flow parameters, this in turn requires correlations for various interfacial and wall interaction effects that are flow regime dependent. For many systems of practical interest, however, the evolution of flow regimes (such as slug flow in oil–gas pipelines) is of interest because the development lengths are long and flow regimes may change in regions where pipeline inclination changes due to the terrain. It is shown here that for slow transients in near-horizontal pipes, the one-dimensional multi-field model, when solved with sufficient resolution, does not require flow regimes to be specified or flow regime dependent closure relationships. The formulation predicts the development of flow regimes and various flow parameters without the need for maps, or the need to change closure relationships. To accomplish this, the model includes four fields, i.e. continuous and dispersed liquid, continuous and dispersed gas, as well as a set of appropriate closure relationships from the literature.

For the main application considered here, i.e. slow transients in oil–gas pipelines, order of magnitude analyses indicate that certain inertial terms in the model are very small and can be neglected in comparison to the others. Advantage is taken of this to simplify both the structure of the mathematical problem and the solution procedure, which is sufficiently accurate that mass is conserved for each of the four fields. Furthermore, the calculations require high spatial resolution, so a fast, easily-parallelizable numerical procedure has been applied.

The results indicate that the development of certain flow regimes, including transitions from bubbly to stratified flow and vice versa, slug flow including slug frequency and length, and the evolution of these parameters along a pipeline are well predicted by the model when compared to experimental data. As part of the validation it is also shown that the model predicts, without need to change closure relationships, flow regimes in fully-developed near-horizontal two-phase flows in good agreement with existing flow regime maps. This suggests that for slow transients in flows for which one-dimensional effects dominate, predictions can be made without requirements for flow regime maps and closure relationships that depend on them.

1. Introduction

Multi-field approaches to modeling two-phase flows have been around for some time, a version being discussed in Wallis's text (Wallis, 1969) as the separate-cylinders model. These models all require some form of averaging for the usual local instantaneous conservation equations, which results in the removal of information regarding gradients in the vicinity of interfaces and boundaries. As a consequence, relationships must be specified to provide information regarding fluxes of the conserved quantities at interfaces and boundaries. Early development of the model was initiated by problems in the nuclear industry (see Vernier and Delhaye (1968), Ishii (1975), Delhaye and Achard (1977), amongst many others). At this time a problem with the model was that it did not retain its hyperbolic form, even for simple flows, leading to high wave number instabilities when calculations were performed by methods that gave rise to low numerical diffusion. This problem was to some extent resolved, in particular for horizontal stratified flows, by Banerjee and Chan (1980), who were able to show that the instabilities arose because of incorrect simplifying assumptions regarding the pressure field. They showed that when gravitational effects on the mean pressure in each phase were properly accounted for, the onset of linear instabilities coincided with the Kelvin–Helmholtz predictions. The well-posedness aspects of this problem was also considered more recently by

* Corresponding author. Tel.: +39 02 55601989; fax: +39 02 55607756.
E-mail address: marco.bonizzi@tea-group.com (M. Bonizzi).

0301-9322/$ - see front matter © 2008 Elsevier Ltd. All rights reserved.
doi:10.1016/j.ijmultiphaseflow.2008.09.001

Louaked et al. (2003) and Holmas et al. (2008). Viscous effects could be important for interfacial instabilities in stratified flows, and were considered by Lin and Hanratty (1986), and Barnea and Taitel (1993), who also considered nonlinear effects in Barnea and Taitel (1994).

At about this time, several attempts were made to use the multifield model to capture flow regime transitions. This was considered desirable because success in this direction would allow the use of closure relationships that were independent of phase distributions (flow regimes) and would simplify calculation procedures. Amongst these attempts, Kawaji and Banerjee (1987) used a two-field formulation that included surface tension to model inverted annular flow during the rewetting process. They were able to predict the lengths of interfacial waves that were in agreement with experiments, and use the model to capture break-up of the liquid core to form droplets. However, such attempts had limited success and flow regime maps and closure relationships dependent on flow regimes continued to be used. An important limitation of such maps is that they are usually based on local flow parameters which make it difficult to predict history effects on flow regimes, a problem that is often important in transients and entrance regimes.

During this early period, several computer codes for analyzing nuclear loss-of-coolant accidents, based on the multifield model, were also developed. Amongst these, the French code CATHARE (Micaelli, 1987) was based on a formulation ensuring that the characteristics were real for each flow regime – but CATHARE still continued to use flow regime maps and closure relationships dependent on them. Several other codes were developed, but these not only used flow regime maps but also did not ensure that the mathematical problem was hyperbolic for each flow regime (e.g., Hall and Johnson (1982)). It appears that the implicit assumption was made that the high wave number instabilities that arose when the characteristics became complex could be damped out numerically without affecting the quality of the results at the lower wave numbers – see also Holmas et al. (2008). (As an aside, this approach is quite similar to what is done for large-eddy simulations with lattice-Boltzmann methods, where it is seen that the pressure noise arising from the slight compressibility of the model only affects very high wave numbers around the Kolmogorov cutoff and has little effect on the inertial sub range eddies). Be that as it may, a similar approach was then followed for transient analysis of oil–gas pipelines by several groups, e.g. Pauchon et al. (1994) and Bendiksen et al. (1991). As mentioned earlier flow regime maps do not capture flow history effects, and since for near-horizontal gas–liquid pipelines the development of slug flows is of particular importance, these approaches had to incorporate some form of explicit slug tracking approach – see Nydal and Banerjee (1996) for an example.

For predominantly one-dimensional flows, much of the important behavior can perhaps be captured by considering continuous and dispersed liquid and gas phases i.e. four fields. For example, slug flow may be thought of as a continuous gas phase, perhaps containing a few drops with the liquid phase intermittently interspersed and containing entrained gas bubbles. Similarly, a stratified flow might be thought of as separated gas and liquid phases, each containing a few drops and bubbles, respectively. Bubbly flow, following this line of thought, would then consist of a continuous liquid phase containing gas bubbles with a negligible continuous gas layer (containing droplets). Furthermore, an annular flow would consist of a continuous gas phase containing liquid droplets and a continuous liquid phase containing gas bubbles, the proportion of continuous liquid being insufficient to bridge the duct while remaining continuous. Obviously, within this one-dimensional context, the distinction between stratified flows and annular flows would be difficult to capture as a consequence of the one-dimensional formulation. It is therefore essential to note that there are many two-phase flow problems that require a multi-dimensional formulation for their elucidation, e.g., churn turbulent flow. Having said this though, there are a significant array of problems of practical interest that could yield to resolution by one-dimensional approaches without the necessity for explicit definition of flow regimes and the closure relationships associated with each of them. The demarcation of such a group of problems is to some extent a matter of taste and depends on the accuracy with which it is desired to predict flow behavior. For the range of problems of interest in near-horizontal pipelines, many of the conditions for use of one-dimensional approaches are met, particularly for relatively slow transients in flow, leaving rapid transients such as due to pipeline rupture or transition from horizontal to vertical pipes out of consideration for the moment.

This discussion then leads to this paper, in which we will develop and apply a four field model consisting of continuous liquid containing dispersed gas bubbles and continuous gas containing liquid droplets. The model will incorporate a representative set of closure relationships which will not be adjusted for changes in flow configuration (i.e. will remain the same throughout the calculations – though of course they will be a function of non-dimensional groups such as the Reynolds number and the Eotvos number, which do not depend on flow regimes but directly on the fluids properties and the dependent variables that are calculated).

This approach implicitly propagates interfacial area, but the area is divided into a continuous component and a dispersed component, associated with the bubbles and drops. The rate of the transport processes that occur at the continuous and dispersed components are of course very different, and the approach captures this naturally.

It should be noted in this introductory section that details of the numerical procedures used are not the subject of this paper, as there are many possibilities that would achieve the performance needed. A key aspect is that it was found to be important to conserve mass for each of the four fields throughout the calculations in order to make good predictions. It was also found that the proposed four-field model could be significantly simplified with regard to the inertial terms for the dispersed phase momentum formulations, as these were always small when compared to the others. This results in the model remaining hyperbolic for the computations, which of course was the key to enabling the use of fine nodalization. Clearly, fine nodalization and calculations performed with Courant numbers ~ 1, as was done here, has the effect of substantially decreasing numerical diffusion. This in turn would destabilize the calculations by giving rise to high wave number instabilities, if the model had complex characteristics. As well, easily parallelizable numerical procedures that enabled the use of fine nodalization for problems of practical interest were desirable.

The sensitivities of the predictions to the closure relationships have not been investigated as far as their effect on the validation of the proposed procedure is concerned. Their precise nature is important to some extent but the main hypothesis of interest for this paper is that a set that are not dependent on flow regimes may be used to give reasonable results. After all we are interested in determining whether the approach will capture first order effects such as the development of flow regimes, the determination of which to some extent lies in the eye of the beholder. In any case, the computational software has been formulated in a manner such that closure relationships can be readily changed, so the sensitivity of the illustrative validations contained in this paper, to the closures adopted, may be checked in the future.

2. The model

In the multi-field model (Ishii, 1975; Chan and Banerjee, 1980 and many others) separate sets of conservation equations are written for each field. In our case, we proceed with four fields, where ε_L, ε_l, ε_d, ε_G, ε_g, ε_b denote the volume fractions of total liquid, of liquid continuous, of liquid dispersed (droplets), of total gas, of gas continuous and dispersed (bubbles), respectively. The following relations hold, since only four fields are independent with the constraint that they must sum to unity for the total liquid and gas volume fractions.

$$\varepsilon_L = \varepsilon_l + \varepsilon_d; \quad \varepsilon_G = \varepsilon_g + \varepsilon_b; \quad \varepsilon_L + \varepsilon_G = 1 \tag{1}$$

For isothermal flow 8 conservation equations are required for the four fields: 4 continuity equations and 4 momentum equations. In our formulation two momentum equations are written for the dispersed liquid and gas respectively. Two other momentum equations are written for fields 1 and 2 (sometimes called layers here) – the former stands for liquid continuous + gas dispersed, and the latter for gas continuous + liquid dispersed. The corresponding volume fractions and densities are:

$$\varepsilon_1 = \varepsilon_l + \varepsilon_b; \quad \rho_1 = \frac{\varepsilon_l\rho_l + \varepsilon_b\rho_g}{\varepsilon_l + \varepsilon_b}; \quad \varepsilon_2 = \varepsilon_g + \varepsilon_d; \quad \rho_2 = \frac{\varepsilon_g\rho_g + \varepsilon_d\rho_l}{\varepsilon_g + \varepsilon_d} \tag{2}$$

The momentum equations are written in terms of the centre of mass velocity of the two mixture fields,

$$u_1 = \frac{c_b\rho_g u_b + (1-c_b)\rho_l u_l}{\rho_1} \tag{3}$$

for field 1, and

$$u_2 = \frac{c_d\rho_l u_d + (1-c_d)\rho_g u_g}{\rho_2} \tag{4}$$

for field 2. In Eqs. (3) and (4) c_b and c_d denote the ratio of the dispersed field volume fraction to the mixture volume fraction of the layer:

$$c_b = \frac{\varepsilon_b}{\varepsilon_b + \varepsilon_l}, \quad c_d = \frac{\varepsilon_d}{\varepsilon_d + \varepsilon_g} \tag{5}$$

With the help of Eq. (2) the momentum equations for fields (or layers) 1 and 2 are written as:

$$\begin{aligned}&\frac{\partial(\varepsilon_1\rho_1 u_1)}{\partial t} + \frac{\partial(\varepsilon_1\rho_1 u_1^2)}{\partial z} + \frac{\partial}{\partial z}\left[\left(\frac{\rho_g\rho_l c_b(1-c_b)\varepsilon_1}{\rho_1}\right)u_{s1}^2\right] \\ &= -\varepsilon_1\frac{\partial P}{\partial z} - \varepsilon_1\rho_1 g\cos(\vartheta)\frac{\partial h}{\partial z} - \varepsilon_1\rho_1 g\sin(\vartheta) + -\frac{\tau_{w1}S_{wp1}}{A} \\ &\quad + \frac{\tau_i S_i}{A} - \Phi_e u_l + \Phi_d u_d + \phi_e u_g - \phi_{de} u_b\end{aligned} \tag{6}$$

$$\begin{aligned}&\frac{\partial(\varepsilon_2\rho_2 u_2)}{\partial t} + \frac{\partial(\varepsilon_2\rho_2 u_2^2)}{\partial z} + \frac{\partial}{\partial z}\left[\left(\frac{\rho_g\rho_l c_d(1-c_d)\varepsilon_2}{\rho_2}\right)u_{s2}^2\right] \\ &= -\varepsilon_2\frac{\partial P}{\partial z} - \varepsilon_2\rho_2 g\cos(\vartheta)\frac{\partial h}{\partial z} - \varepsilon_2\rho_2 g\sin(\vartheta) + -\frac{\tau_{w2}S_{wp2}}{A} \\ &\quad - \frac{\tau_i S_i}{A} + \Phi_e u_l - \Phi_d u_d - \phi_e u_g + \phi_{de} u_b\end{aligned} \tag{7}$$

The notation in these equations is: z and t are the spatial and temporal coordinates, subscripts 1, 2, s_1, s_2 l, g, d, and b denote field 1, field 2, slip between bubbles and continuous liquid, slip between droplets and continuous gas, liquid continuous and gas continuous field, and droplets and bubbles field respectively. ε denotes the volume fraction, u is the velocity, g is the gravity acceleration, P is the interfacial pressure, h the liquid height, τ is the shear stress, ρ the density, A is the pipe area, ϑ is the pipe inclination with respect to the horizontal, S_{wp1}, $S_{wp2}$and S_i denote the perimeter wetted by layer 1, the perimeter wetted by layer 2, and the interfacial width respectively. As shown in the Appendix, the last two terms on the LHS of Eqs. (6) and (7) involving the slip are very small compared to the other terms on the LHS.

The wall shear stress is typically expressed as:

$$\tau_{wk} = \frac{1}{2}f_{wk}\rho_k|u_k|u_k \tag{8}$$

where f_{wk} denotes the wall friction factor while the subscript k denotes the phase in contact with the wall, i.e. u_g if it is the gas and u_l if it is the liquid. Similarly, the interfacial shear stress is expressed as:

$$\tau_i = \frac{1}{2}f_i\rho_g|u_g - u_l|(u_g - u_l) \tag{9}$$

The source terms ϕ_e, ϕ_{de}, Φ_e and Φ_d denote bubble entrainment and disengagement rates, and droplet entrainment and deposition rates respectively. The velocities of the dispersed fields (u_d – droplet velocity, and u_b –bubble velocity) are calculated from the momentum equations written for the dispersed phase equations. The momentum equations for the dispersed fields may be written as

$$\begin{aligned}\frac{\partial(\varepsilon_m\rho_m u_m)}{\partial t} + \frac{\partial(\varepsilon_m\rho_m u_m^2)}{\partial z} &= -\varepsilon_m\frac{\partial P}{\partial z} - \varepsilon_m\rho_m g\sin(\vartheta) + \Omega_e u_k \\ &\quad + \Omega_{de}u_m + F_{\text{drag}}\end{aligned} \tag{10}$$

In this equation, subscript m denotes the dispersed field (i.e. drops or bubbles), Ω_e and Ω_{de} denote the entrainment and disengagement rates for the given dispersed field (i.e. droplet entrainment/deposition for the dispersed liquid field and gas entrainment rate and disengagement, like shedding from the slug tail for bubbles). F_{drag} is the interfacial drag acting on the dispersed field. The order of magnitude of each of the terms on the LHS of Eq. (10), as well as the virtual mass, the Basset force, the lift force and hydraulic head terms are small in our scenarios of interest compared to each term on the RHS. This has been validated on the basis of a posteriori evaluations. So Eq. (10) leads to essentially algebraic equations, which do not alter the characteristics and which remain real.

The mass conservation equations of the four fields (liquid continuous, liquid dispersed, gas continuous, and gas dispersed) are:

$$\frac{\partial(\varepsilon_l\rho_l)}{\partial t} + \frac{\partial(\varepsilon_l\rho_l u_l)}{\partial z} = -\Phi_e + \Phi_d \tag{11}$$

$$\frac{\partial(\varepsilon_d\rho_l)}{\partial t} + \frac{\partial(\varepsilon_d\rho_l u_d)}{\partial z} = \Phi_e - \Phi_d \tag{12}$$

$$\frac{\partial(\varepsilon_g\rho_g)}{\partial t} + \frac{\partial(\varepsilon_g\rho_g u_g)}{\partial z} = -\phi_e + \phi_{de} \tag{13}$$

$$\frac{\partial(\varepsilon_b\rho_g)}{\partial t} + \frac{\partial(\varepsilon_b\rho_g u_b)}{\partial z} = \phi_e - \phi_{de} \tag{14}$$

The mass conservation equations for the total liquid and gas volume fractions are obtained by summing Eqs. (11)–(14) respectively:

$$\frac{\partial(\varepsilon_L\rho_l)}{\partial t} + \frac{\partial(\varepsilon_l\rho_l u_l)}{\partial z} + \frac{\partial(\varepsilon_d\rho_l u_d)}{\partial z} = 0 \tag{15}$$

$$\frac{\partial(\varepsilon_G\rho_g)}{\partial t} + \frac{\partial(\varepsilon_g\rho_g u_g)}{\partial z} + \frac{\partial(\varepsilon_b\rho_g u_b)}{\partial z} = 0 \tag{16}$$

In order to close the set of equations described above, it is necessary to incorporate the necessary closure relationships for the quantities on the right hand side of the conservation equations. These include friction factors for the computation of the shear stresses (τ_{wk}, τ_i, τ_{drag}), terms related to mass exchange (e.g. droplet entrainment rate Φ_e droplet deposition rate Φ_d and gas entrainment and disengagement rates ϕ_e and ϕ_{de} respectively).

For purposes of validation, we will determine whether some of the so-called "flow regimes" are predicted as part of the results obtained when conducting the calculation. This requires that a set of criteria be defined as to what constitutes a "flow regime" for identification purposes only. These are not needed as part of the calculation but only as part of the validation procedures proposed here. Thus they are not shown as part of the section on closure relationships but only in the section on validation of the model.

3. Closure relationships

We summarize here the closure relationships used in this paper. They are independent of flow regime. The numerical procedures have been structured such that users may change and/or adjust the closures. Tables 1–3 report all the empirical closures required by the model. In particular, Table 1 lists the reference closures for the wall and interfacial friction factors. This is followed by Table 2 which reports the correlations adopted for rough pipe wall and summarizes alternative correlations for the wall and interfacial friction factors that have been used to test the sensitivity of the flow regime predictions. Table 3 summarizes the reference closures used for bubble entrainment and disengagement, droplet entrainment and deposition, droplet size and bubble size, drag coefficients for drops and bubbles.

In Table 1 the following nomenclature has been used:

$$Re_l = \frac{\rho_k u_k D_k}{\mu_k}, Re_{sl} = \frac{\rho_l U_{sl} D}{\mu_l}, Re_i = \frac{\rho_g |u_g - u_l| D_2}{\mu_g} \tag{17}$$

Where k stands for either continuous liquid or gas and U_{sl} denotes the liquid superficial velocity. The hydraulic diameters are defined as

$$D_1 = \frac{4A_1}{S_{wp1}}, D_2 = \frac{4A_2}{S_{wp2} + S_i} \tag{18}$$

In the expression of Andreussi and Persen (1987) the coefficient F is defined as:

$$F = (u_g - u_l)\sqrt{\frac{\rho_g}{\rho_l - \rho_g}\frac{\frac{dA_1}{dh_1}}{A_2}\frac{1}{g\cos\vartheta}} \tag{19}$$

where, in Eq. (19) F represents a parameter related to the inviscid Kelvin-Helmholtz instability.

In Table 3 u_{wave} denotes the wave celerity; σ_{gl} denotes the gas–liquid surface tension; the coefficient K in the bubbles disengagement law is taken as 0.28; the deposition velocity k_d is taken to be 0.1 m/s; the droplets entrainment constant k_e is taken to be 7.7e-8. The droplets and bubbles Reynolds numbers and the Eotvos number are defined as

Table 1
Reference closure relationships for friction factors

Closure	Reference	Condition	Equation
Liquid-wall	Taitel and Dukler (1976)	$Re_l < 2100$	$f_{lw} = 16/\mathrm{Re}_l$
		$Re_l \geqslant 2100$	$f_{lw} = 0.046[Re_l]^{-0.2}$
Gas-wall	Taitel and Dukler (1976)	$Re_g < 2100$	$f_{gw} = 16/\mathrm{Re}_g$
		$Re_g \geqslant 2100$	$f_{gw} = 0.046[Re_g]^{-0.2}$
Gas–liquid	Taitel and Dukler (1976)	$\mathrm{Re}_i < 2100$	$f_i = 16/Re_i$
		$\mathrm{Re}_i >= 2100$	$f_i = 0.046[Re_i]^{-0.2}$

Table 2
Additional relationships for friction factor

Closure	Reference	Condition	Equation
Liquid-wall	Spedding and Hand (1997)	$Re_l < 2100$	$f_{lw} = 24/\mathrm{Re}_l$
		$Re_l \geqslant 2100$	$f_{lw} = 0.0262[\varepsilon_1 Re_{Sl}]^{-0.139}$
Liquid-wall	Moody (Hall, 1957)	$Re_l < 2100$	$f_{lw} = 16/\mathrm{Re}_l$
		$Re_l \geqslant 2100$	$f_{lw} = .001375\left[1 + \sqrt[3]{\left(\frac{2\cdot 10^4 \cdot k}{D_1} + \frac{10^6}{Re_l}\right)}\right]$
Gas-wall	Moody (Hall, 1957)	$Re_g < 2100$	$f_{gw} = 16/\mathrm{Re}_g$
		$Re_g \geqslant 2100$	$f_{gw} = .001375\left[1 + \sqrt[3]{\left(\frac{2\cdot 10^4 \cdot k}{D_2} + \frac{10^6}{Re_g}\right)}\right]$
Gas–liquid	Andreussi and Persen (1987)	$F \leqslant F_0 = 0.36$	$f_i = f_{gw}$
		$F > F_0 = 0.36$	$f_i = f_{gw}\left[1 + 29.7(F - 0.36)^{0.67}\left(\frac{h_1}{D}\right)^{0.2}\right]$
Gas–liquid	Andritsos and Hanratty (1987)	$\varepsilon_2 u_2 < U_{G,\mathrm{crit}} = 5\sqrt{\frac{\rho_g(P_{atm})}{\rho_g(P)}}$	$f_i = f_{gw}$
		$\varepsilon_2 u_2 \geqslant U_{G,\mathrm{crit}} = 5\sqrt{\frac{\rho_g(P_{atm})}{\rho_g(P)}}$	$f_i = f_{gw}\left(1 + 15\sqrt{\frac{h_1}{D}}\left(\frac{u_2\varepsilon_2}{U_{G,\mathrm{crit}}} - 1\right)\right)$
Gas–liquid	Cohen and Hanratty (1968)	None	$f_i = 0.014$
Gas–liquid	Wallis (1969)	None	$f_i = 0.005[1 + 75\varepsilon_1]$

Table 3
Other required closures for multi-field model

Closure relationship	Reference	Equation
Bubble Entrainment	Nydal and Andreussi (1991)	$\phi_e = \rho_g A\left[0.076\frac{S_i}{D}(u_{wave} - u_l) - 0.15\right]$
Bubble Disengagement	Andreussi et al. (1993a,b)	$\phi_{de} = -\rho_g K\left[1.18\left(\frac{\sigma_{gl} g(\rho_l - \rho_g)}{\rho_l^2}\right)\right]^{0.25} S_i(1 - \varepsilon_l)$
Droplet entrainment rate	Pan and Hanratty (2002)	$\Phi_e = \frac{4}{\pi D}\frac{k_e}{\sigma_{gl}}\sqrt{\rho_g\rho_l}u_g^2\left(\frac{\rho_l A u_l \varepsilon_l}{D} - 100\mu_l\right)$
Droplet deposition rate	Pan and Hanratty (2002)	$\Phi_d = \frac{4}{D}k_d\frac{\varepsilon_d}{\varepsilon_g}\rho_l$
Drag on droplet	Alipchenkov et al. (2004)	$C_D = \frac{18.5}{\mathrm{Re}_d^{0.6}}, 2 < \mathrm{Re}_d < 500$
		$C_D = 0.44, \mathrm{Re}_d > 500$
Droplet diameter	Sarkhi and Hanratty (2002)	$d_d = \frac{1}{U_{sg}^{1.1}}\left[4.848\frac{\pi\Phi_g D}{\rho_l U_{sg}} + 0.0038\right]$
Drag on bubble	Tomiyama et al. (1995)	$C_D = \max\left[\frac{24}{Re_b}\left(1 + 0.15\cdot Re_b^{0.687}\right), \frac{8}{3}\frac{Eo}{Eo+4}\right]$
Bubble diameter	Andreussi et al. (1999)	$d_b = \frac{\sigma_{gl}}{\frac{1}{2}f_{lw}\rho_l u_i^2} We_{\mathrm{crit}}^0\left(1 + 51.7\varepsilon_b^{1.5}\right), We_{\mathrm{crit}}^0 = 1.05$

$$Re_d = \frac{\rho_g |u_g - u_d| d_d}{\mu_g}, Re_b = \frac{\rho_l d_b |u_1 - u_b|}{\mu_l}, Eo = \frac{g(\rho_l - \rho_g) d_b^2}{\sigma_{gl}} \quad (20)$$

with d being the droplet average diameter.

From Table 1 it can be seen that, as a first option, the closure equations first proposed by Taitel and Dukler (1976) for the wall and interfacial friction factors under stratified flow conditions have been adopted. This choice has been widely used in the literature and appears to be adequate when dealing with low phase velocities, in the absence of interfacial waves. Table 2 lists the wall friction factors used in the model in presence of a rough wall. These correlations are the standard, turbulent flow equations normally adopted for the computation of frictional losses in single-phase pipe flow. In the same table, we also list a limited number of correlations proposed in the literature to account for the effect of the interfacial roughness on the liquid-wall friction factor and on the interfacial friction factor. In these cases the number of possible choices is large. The closure equations reported in Table 3 are not yet well established, mainly because of the lack of extensive data sets and improvements will require new data. We decided to postpone any detailed comparison among the different correlations and with the experimental measurements, as the main objective of the present paper is to determine the applicability of the four-field model with an appropriate set of closure relationships in the prediction of flow structure development and transition. To this it may be added that, in general, the in the studies we have conducted, the effect of the closure equations was quite limited.

4. Numerical procedures, mass error and convergence

The mass conservation equations solved are Eqs. (12) and (14) for the liquid and gas dispersed fields and Eqs. (15) and (16) for the total liquid and gas volume fractions. Once these equations are solved, the volume fractions of the continuous fields can be calculated applying Eq. (1):

$$\varepsilon_l = \varepsilon_L - \varepsilon_d, \quad \varepsilon_g = \varepsilon_G - \varepsilon_b \quad (21)$$

The pressure equation is derived by combining the mass equations for the conservation of the total liquid and gas, and dividing by the respective densities, the derived equation being:

$$\frac{1}{\rho_l}\left[\frac{\partial(\varepsilon_l \rho_l u_l)}{\partial z} + \frac{\partial(\varepsilon_d \rho_l u_d)}{\partial z}\right] + \frac{1}{\rho_g}\left[\frac{\partial(\varepsilon_g \rho_g u_g)}{\partial z} + \frac{\partial(\varepsilon_b \rho_g u_b)}{\partial z}\right] + \frac{\varepsilon_G}{\rho_g}\frac{\partial \rho_g}{\partial t} + \frac{\varepsilon_L}{\rho_l}\frac{\partial \rho_l}{\partial t} = 0 \quad (22)$$

A standard pressure-velocity coupling scheme (Ferziger and Peric, 1999) is the choice adopted to derive a pressure equation from the global continuity Eq. (22).

The governing equations are numerically discretized on a staggered grid arrangement (Harlow and Welch, 1965) using explicit discretization scheme in time for all equations but the pressure. The adoption of the explicit scheme allows easier parallelization. The time step is limited by the flow Courant number

$$C = \frac{u_{\max} \delta t}{\delta z} < 1. \quad (23)$$

In the above equation C, u_{max}, δt and δz denote the Courant number, the maximum phase velocity, the time step size and the mesh spacing respectively.

Since the set of model equations is hyperbolic, the boundary conditions have to be prescribed by the characteristics velocity in and out of the flow.

In summary, the methodology solves the following equations:

1. Momentum equation of layer 1 – Eq. (6) [explicitly integrated].
2. Momentum equation of layer 2 – Eq. (7) [explicitly integrated].
3. Momentum equations for the dispersed phases – Eq. (10) [explicitly integrated].
4. Continuity equation of liquid dispersed (droplet) field – Eq. (12) [explicitly integrated].
5. Continuity equation of gas dispersed (bubbles) field – Eq. (14) [explicitly integrated].
6. Continuity equation of total liquid phase – Eq. (15) [explicitly integrated].
7. Continuity equation of total gas phase – Eq. (16) [explicitly integrated].
8. The pressure equation derived Eq. (22) [implicitly integrated].

If inlet conditions are stratified, a small disturbance needs to be imposed in order to initiate evolution to the appropriate flow configuration. If the flow is truly stratified, then these disturbances die out to the level of numerical noise in the void fraction fluctuations. However, if transition to slug or large-wave (annular) flow would occur, then these fluctuations grow to significant and sustained amplitude. In discussing the validation of the model it should be kept in mind that when inlet and initial conditions are stratified then small amplitude fluctuations are imposed to assist in flow evolution.

The procedure enforces mass conservation of not only the total liquid and gas phases, but also that of the corresponding dispersed fields (gas bubbles and liquid droplets). At any instant in time, the following equation holds:

$$\sum_{k=0}^{p=N} \left(\dot{M}_{\text{out}}(t_p) - \dot{M}_{\text{in}}(t_p)\right)\delta t_p = (M(t_N) - M(t_0)) \quad (24)$$

In the above equation subscript p represents a time step in the numerical solution. The term in the left hand side of (24) denotes the difference between the outlet and inlet masses for the field under consideration, while the term in the right hand side represents the accumulation term.

As an example of mass conservation capabilities of the numerical method, a transient case is considered for illustrative purposes. Air-water stratified flow is fed into a horizontal line (30 m long with an internal diameter of 8 cm) at atmospheric pressure. The superficial velocities of the gas and liquid are of 3 and 0.2 m/s respectively. With these boundary conditions, stratified flow is expected based on the normal flow regime maps (Taitel and Dukler, 1976). At a certain time (120 s from the start of the simulation) the liquid flow rate is ramped up from 0.2 to 0.5 m/s, while the gas flow rate is kept constant. The increase in liquid velocity should be enough to lead to hydrodynamic slugging in the line (Taitel and Dukler, 1976). We now consider the simulation performed with a mesh spacing of one pipe diameter and a Courant number of 0.2. The cumulative mass errors for the total liquid and gas during the transient simulation are displayed in the Fig. 1. Despite the increase in liquid flow rate, the mass errors for both the total liquid and gas phases remain low, always <1%. The dispersed gas field accumulates a mass error totally negligible (less than E-7 %).

With regards to convergence of the numerical results, consider the results shown in Fig. 2 for the effect of the mesh size on the slug frequency for a terrain-induced slugging case occurring in a V-section operating at high pressure. It is evident that when the mesh size is reduced to the size of the diameter the numerical predictions become grid-independent. This effect is due to the diminished effect of numerical diffusion which, as the grid becomes coarser, tends to smear out sharp changes in the solution (i.e. it smoothes out slug fronts and large disturbance waves). Clearly convergence of the calculations should be checked, but in rough terms is obtained with mesh spacings of the order of the pipe diameter as demonstrated by the demanding case considered.

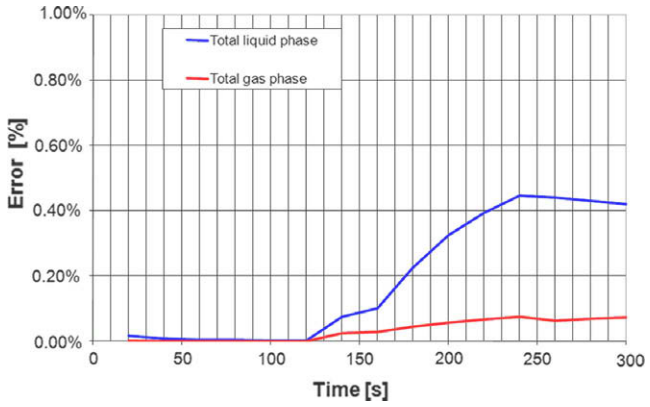

Fig. 1. Cumulative mass errors for total liquid and gas phases.

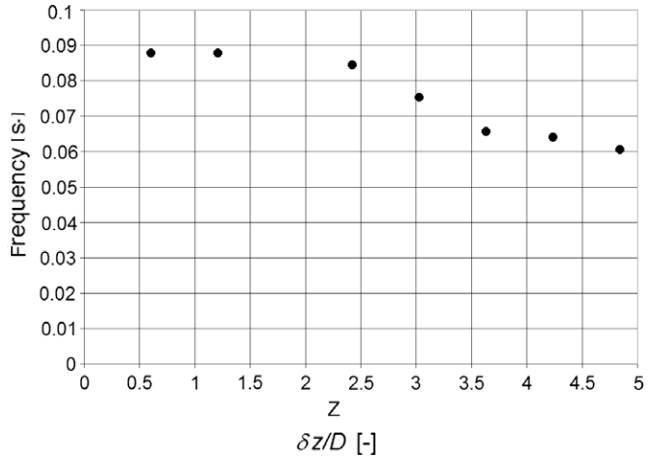

Fig. 2. Slug frequency vs. non-dimensional mesh spacing.

5. Validation of the model

5.1. Criteria for identification of flow regimes

The validation will focus on determining the capabilities of the four-field model with closure relationships independent of flow regimes on prediction of qualitative changes in phase distribution (i.e. prediction of flow regimes). For these purposes we require criteria to identify the specific flow regimes noting that these play no role in the calculation of the closure relationships utilized. Thus not only are the fully developed flow regimes predicted but also the evolution of the phase distributions towards their steady-state configurations. For example, we may start with conditions along the pipe of dispersed bubbly flow but, based on steady-state fully-developed flow regime maps, we know that the inlet flow conditions should result in stratified flow. Indeed our calculations will show that the dispersed bubbly flow will evolve ultimately to a stratified flow. Similarly, we may start with inlet conditions which for a fully developed case should lead to slug flow but are considered initially to be stratified. Our calculations again will show that such initially stratified flows will develop into slugs with appropriate length and frequency. Clearly, this requires criteria to identify what is a slug for the purposes of validation noting that the model and its solution does not require any such criteria. We therefore list below the criteria used for identification of the various flow regimes. The results of course are rather insensitive to the precise values of the thresholds used in these criteria as flow regimes are a qualitative determination of phase distribution. Qualitatively we define

- Stratified flow: stratified layers with low void fraction fluctuations (no distinction is made between wavy and smooth regimes).
- Annular flow: stratified layers with large void fraction fluctuations which do not bridge the pipe.
- Slug flow: stratified layers with large void fraction fluctuations which do bridge the pipe, causing regions with very thin stratified gas layers.
- Bubbly flow: the pipe is fully bridged with no regions where there are stratified gas layers that are not very thin.

The term 'very thin stratified gas layer' requires more precise definition for identification purposes. Consider first transition from a stratified flow to a slug flow. The criteria are rather simple. When a wave becomes large enough to reach the top of the pipe then a slug might be thought to form, i.e. the volume fraction of the continuous gas must become very small. Similarly the change of the volume fraction of whatever gas remains must also be small. The exigencies of the numerical procedures require that these volume fractions for the continuous gas layer be slightly greater than zero, but of course the precise values chosen should not matter. Thus we have $\Delta\varepsilon_g \leqslant c_1$ and $\varepsilon_g \leqslant c_2$ where c_1 and c_2 are close to zero, but can be varied over a range without affecting the results. This is shown in the following paragraph.

For transition from slug to bubbly flow the slug lengths become long enough to encompass the whole length of the pipe. Conversely, a bubbly flow becomes a slug flow when the bubbles disengage to add to the stratified gas layer (which could contain very small numbers of liquid droplets) leading eventually to intermittent gas and liquid layer flow.

5.2. Validation for transition from stratified to slug flow

The growth of an interfacial disturbance in stratified flow is shown in Fig. 3 which indicates the liquid volume fraction and the gas velocity at different times for a 30 m long horizontal line, 80 mm internal diameter, operating at atmospheric pressure. The inlet oil ($\rho_L = 820$, $\mu_L = 0.01$ Pa · s) and air superficial velocities are 0.3 and 8 m/s. As can be seen from this figure, the interfacial disturbance grows along the pipeline and rapidly assumes the typical shape of a large disturbance wave as observed in laboratory experiments: a sharp front and a slowly decaying tail. Under these flow conditions the wave grows to the top of the pipe and forms a slug. Immediately before slug formation the gas velocity reaches a peak which in one of the snapshots presented is close to 90 m/s. It is interesting to notice that under these conditions immediately after slug formation a deep trough is formed in the slug tail. Similar experimental observations have been reported in the literature (see for instance, Kadri et al., 2007). Note that all this is predicted without the requirement of any closure relationships specifically for slug flow.

This also regards the elongated bubble propagation velocity for slug flow. In Fig. 4 the correlation based on the experimental observations made by Bendiksen (1984) are compared with the predictions of the present model. According to Bendiksen (1984), the bubble propagation velocity can be written as:

$$u_B = C_0 u_{\mathrm{mix}} + u_0 \tag{25}$$

Bendiksen (1984) proposed the following correlation for his experimental observations:

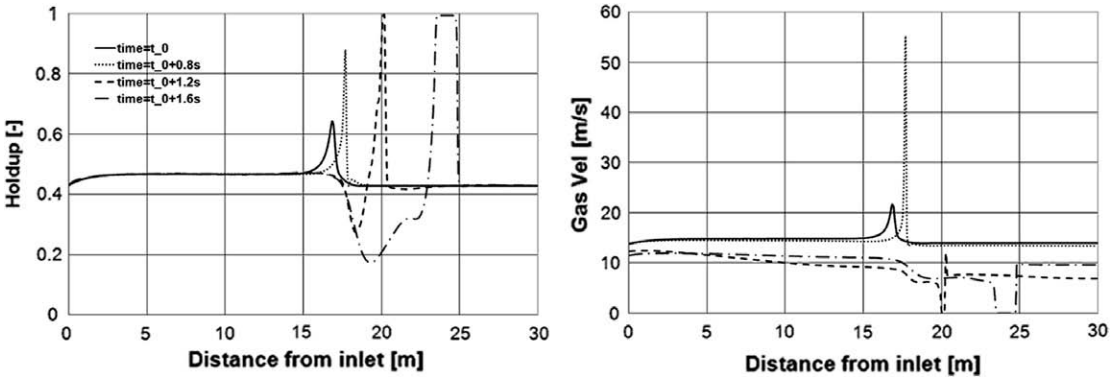

Fig. 3. Liquid holdup and gas velocity profiles at different times (hydrodynamic slugging).

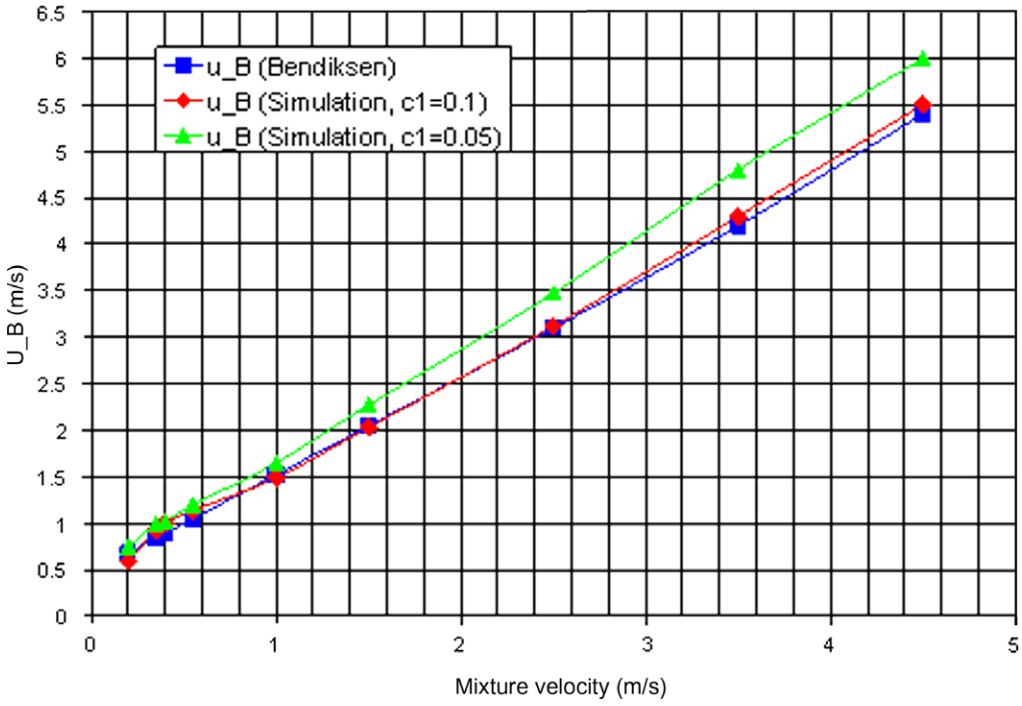

Fig. 4. Bubble velocity in a horizontal line (air-water flow at high pressure in a 3″ pipe).

$$C_0 = \begin{cases} 1.05 + 0.15\sin^2\vartheta & Fr \leqslant 3.5 \\ 1.2 & Fr > 3,5 \end{cases} \tag{26}$$

$$u_0 = \begin{cases} (0.35\sin\vartheta + 0.54\cos\vartheta)\sqrt{gD} & Fr \leqslant 3.5 \\ 0.35\sqrt{gD}\sin\vartheta & Fr > 3,5 \end{cases} \tag{27}$$

In Eqs. (26) and (27) the Froude number is defined as

$$Fr = \frac{u_{\mathrm{mix}}}{\sqrt{gD}} \tag{28}$$

More recent experimental observations (see for instance Nydal et al., 1992) indicate that the value of the coefficient C_0 actually is larger than 1.2 and is closer to 1.25. Fig. 4 compares the bubble velocity according to Eqs. (25)–(27) against the predictions of the four field model using two different values of the criterion thresholdc_1. As can be seen from this figure, a significant change of c_1 causes only a minor change to the gas bubble velocity as would be expected from the previous discussion. It can also be seen that the present model reproduces very well the experimental measurements of Bendiksen (1984) as well as the new data. The main finding here is that no adjustments to the various closure relationships for the four-field model are required to achieve this agreement which is also rather insensitive to the identifications criteria.

Table 4
Effect of threshold values c_1 and c_2 on slug velocity coefficient

C[-]	1.204	1.238	1.316	1.454	1.461	1.415	1.261	1.238
C_1	0.1	0.1	0.1	0.1	0.0125	0.025	0.05	0.15
C_2	0.05	0.04	0.03	0.02	0.04	0.04	0.04	0.04

The effects of the threshold values c_1, c_2 on the slug velocity coefficient C_0 defined by Eq. (26) and empirically fitted by Bendiksen (1984) with Eqs. (26) and (27) are reported in Table 4. This table confirms that the overall effects of the threshold parameters are modest. For instance, a variation of c_1 from 0.0125 to 0.15 only causes a variation of C_0 of less than 20%.

Another interesting example of the effectiveness of the present model in describing slug flow is the prediction of the slug length. In the literature there are no established correlations for this

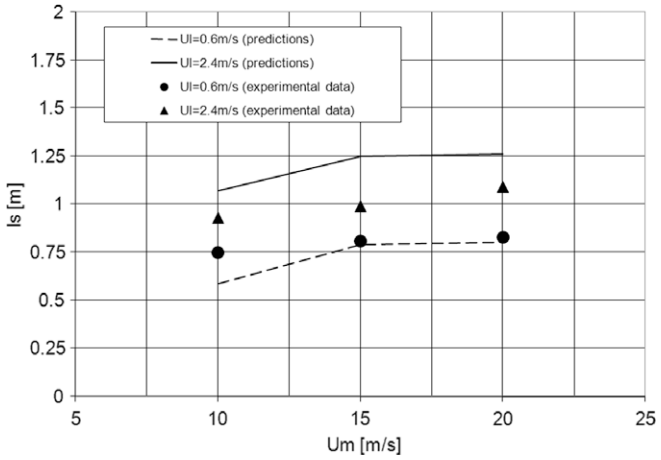

Fig. 5. Comparison between code predictions and experiments for mean slug body length.

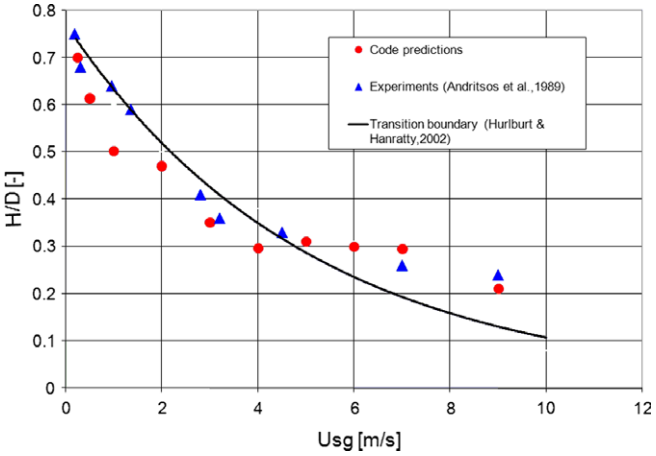

Fig. 7. Air–water theoretical predictions, transition data and predictions.

parameter or for the slug frequency, which can be related to the slug length according to the slug unit model of Dukler and Hubbard (1975). This prevents existing codes, used to predict the main flow parameters in hydrocarbon transportation lines, from providing a reliable estimate of the maximum slug length at pipeline exit. The capability of the present model to predict the slug length is shown in Fig. 5 where model predictions are compared with the experimental observations of Nydal et al. (1992). These authors conducted experiments at atmospheric pressure on horizontal air-water slug flow in pipes having internal diameters of 5 and 9 cm. Numerical simulations were performed for a pipe with internal diameter of 5 cm. Three different mixture velocities (10, 15 and 20 m/s) were considered. For each mixture velocity, two different values of water superficial velocity (0.6 and 2.4 m/s) were examined (the gas superficial velocity changing accordingly). As can be seen from this figure, model predictions are good if it is considered that in this case no data fitting has been performed and no adjustment has been made to the closure relationships. In Fig. 6 the values of the standard deviation of the slug length determined by Nydal et al. (1992) are compared with model predictions and the results obtained again appear to be good in view of the lack of "tuning" in our four-field model.

The robustness of the criteria for identifying the slug transition can also be appreciated by looking at Fig. 7, where the predictions of the critical height of the liquid layer at the transition to slug flow for an air-water flow at atmospheric pressure are plotted against the superficial velocities and compared against the experimental data of Andritsos et al. (1989) and the theoretical transition boundary according to Hurlburt and Hanratty (2002) for a horizontal pipe with 9.53 cm of internal diameter. Clearly, the criteria used for identification, again noting that the closure relationships are not adjusted, appear to be accurate.

Another example is shown in Fig. 8 which plots, for a gas superficial velocity of 6 m/s, the behaviour of the liquid fractions (the liquid height) at a downstream point for two different liquid superficial velocities. As can be seen, at a liquid velocity of 0.15 m/s no slugs are present, but the gas–liquid interface is covered with high frequency, low amplitude noise. With a relatively small change, the liquid velocity goes to 0.2 m/s a well defined train of low frequency (less than 0.05 s-1) slugs can be observed.

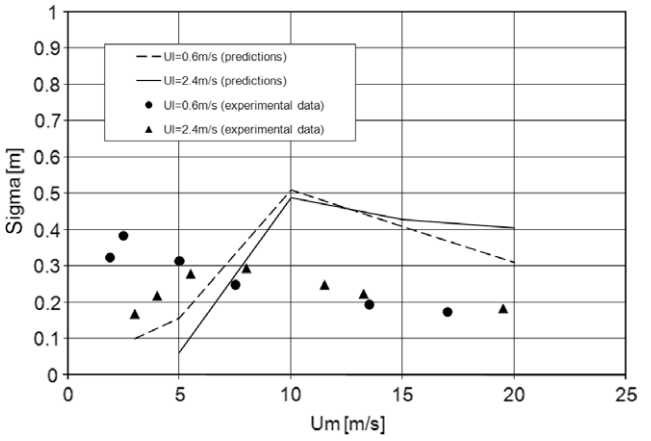

Fig. 6. Comparison between the code predictions and experiments for standard deviations of mean slug length.

5.3. Transition to annular flow

The model predicts the growth of waves between the liquid and gas layers which may either lead to slugging or to the generation of large amplitude waves which do not bridge the pipe and correspond to the onset of annular flow.

As an example Fig. 9 shows the liquid volume fraction (in terms of liquid height) at a downstream point for two different gas superficial velocities (20 and 21 m/s) at a liquid superficial velocity of 0.1 m/s in a horizontal pipe at atmospheric pressure with internal diameter of 9.53 m for a two-phase air-water flow. As can be seen, while the gas–liquid interface remains flat for the lower gas velocity, when this is increased, a train of waves generates. This is predicted again keeping the set of closure relationships unchanged. It is worth noting that the values of wave frequency and height found are in good agreement with the experimental observations (see for instance Lioumbas et al., 2005).

The direct transition between annular and slug flow is shown in Fig. 10, where it can be seen that for a liquid velocity of 0.5 m/s and a gas velocity of 26 m/s the stable flow pattern is annular flow. When the gas velocity is decreased to 17 m/s the stable flow pattern is slug flow.

5.4. Transition to bubbly flow

The transition criterion leading to slug flow formation also allows prediction of the transition to bubbly flows. As discussed bubbly flow is considered to form when the slug frequency is so high that all slugs merge together. As an example, a two-phase flow in a 50 m long pipe with an internal diameter of

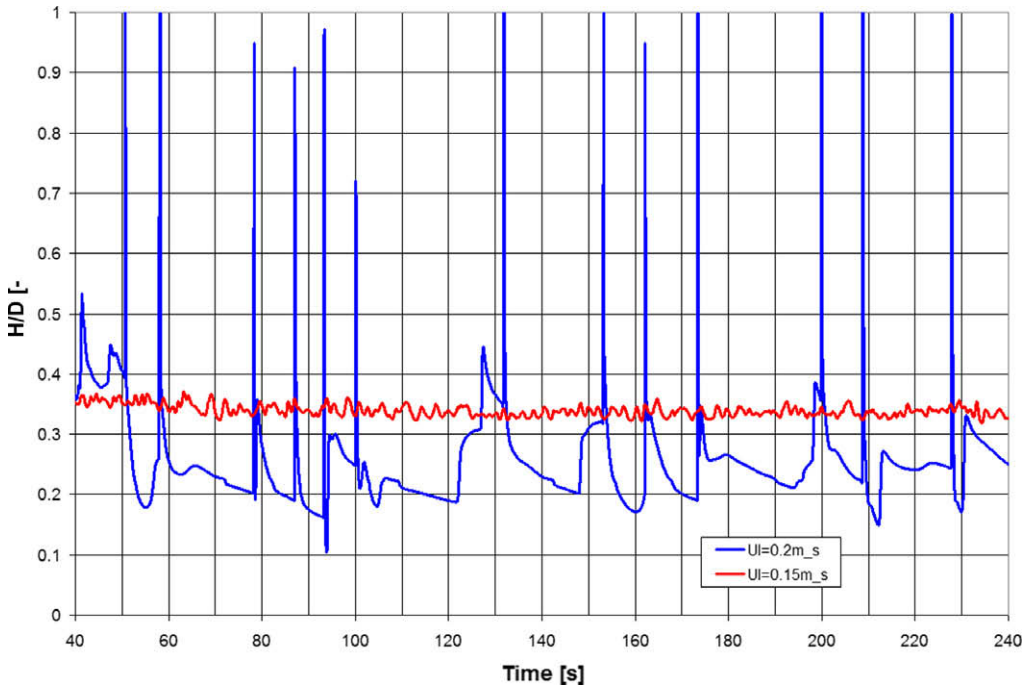

Fig. 8. Liquid height trends in a location close to the exit of a horizontal line at Ug = 6 m/s and different liquid flow rates (blue: $U_l = 0.15$ m/s, red: $U_l = 0.2$ m/s). (For interpretation of the references to colour in this figure legend, the reader is referred to the web version of this article.)

9 cm at atmospheric pressure is studied with inlet superficial velocities of 1 m/s and 10 m/s for the gas and the liquid respectively. The inlet is kept separated with a liquid holdup of 0.2 and the flow is initialized as stratified throughout the line with a liquid holdup of 0.1. After a few seconds the high liquid velocity leads to slug generation at such a high frequency that all bodies merge into a single slug body, as shown in the figure below. As one can see from Fig. 11, a stratified region still exists for some time after the slug is first formed. The same transition can be obtained by changing the inlet boundary conditions, where instead of feeding the gas and liquid as separated, a dispersed gas–liquid flow is fed into the pipe at a mixture velocity of 11 m/s with an inlet bubble voidage of 0.1. Except for the inlet the flow is initialized as stratified, with a liquid holdup of 0.1. Of course the flow should all eventually be bubbly. Fig. 12 shows how this comes about with the inlet boundary condition of dispersed gas–liquid flow propagating downstream along the line. The model predicts that after 16 s from the start of the simulation the whole line is under bubbly flow conditions.

Another interesting numerical exercise was the simulation of a dispersed bubbly flow at the inlet of the pipe at low mixture

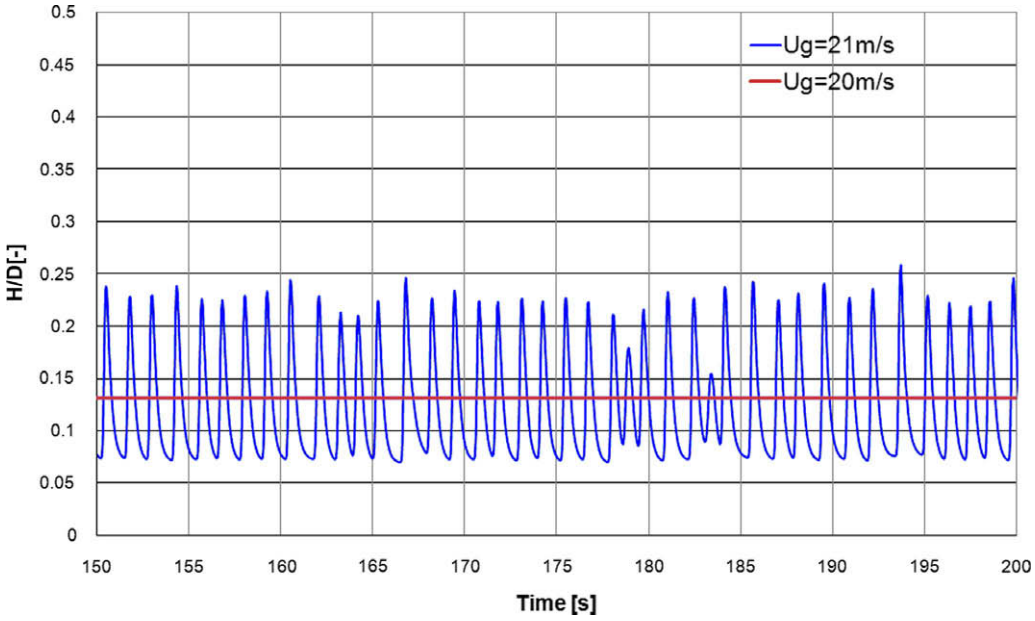

Fig. 9. Transition to annular flow in a horizontal pipe for air-water two-phase flow with liquid velocity of 0.1 m/s and gas velocities of 20 and 21 m/s.

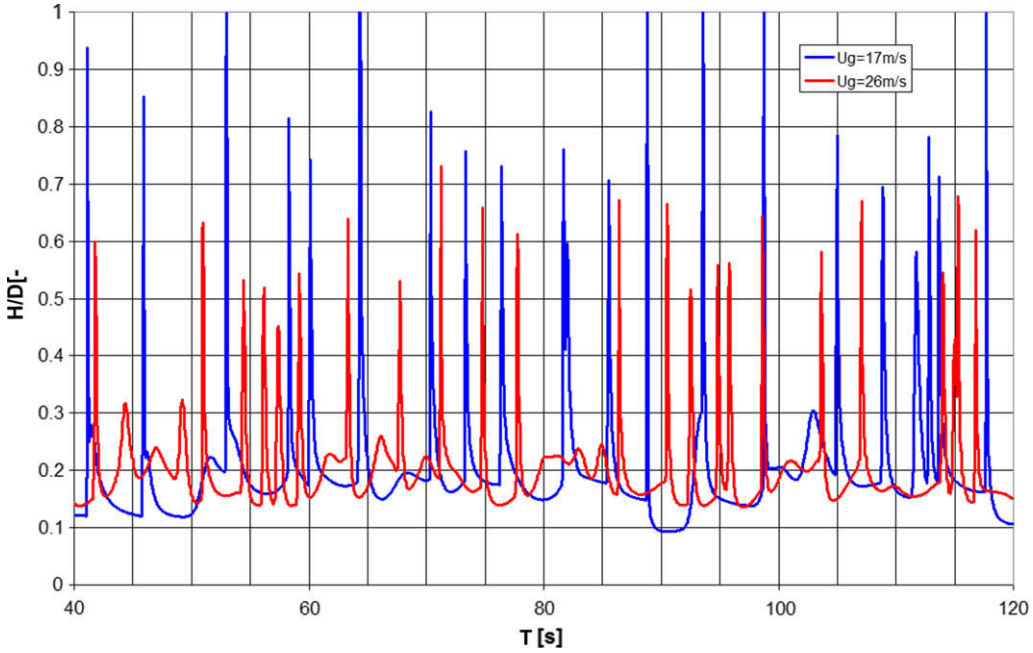

Fig. 10. Transition between Large Waves and Slug flow at Ul = 0.5 m/s (blue: Ug = 17 m/s, red: Ug = 26 m/s). (For interpretation of the references to colour in this figure legend, the reader is referred to the web version of this article.)

velocity (0.1 m/s). The flow is initialized as dispersed throughout the pipe. When the simulation starts, the gas starts to disengage until a stratified flow with a liquid layer containing no bubbles is eventually obtained, as it is expected at such low velocity from existing flow pattern maps (Taitel and Dukler, 1976). Fig. 13 shows the bubbles disengagement as function of time.

5.5. Validation against existing flow regime maps

The flow transitions identified with the present model are summarized in Fig. 14, which refers to a horizontal, 80 mm ID pipe 30 m long, with air and water flowing at atmospheric conditions. In Fig. 14 present results are compared with the flow map proposed by Taitel and Dukler (1976), which is known to provide a good fit to the experimental observations of Mandhane et al. (1974) and to other published work. The good comparison between the two different approaches to predict flow regime transitions shown in the figure indicates not only the validity of the approach presented here but also the importance and accuracy of the mechanistic approach to the problem of flow transitions proposed by Taitel and Dukler (1976) more than 30 years ago.

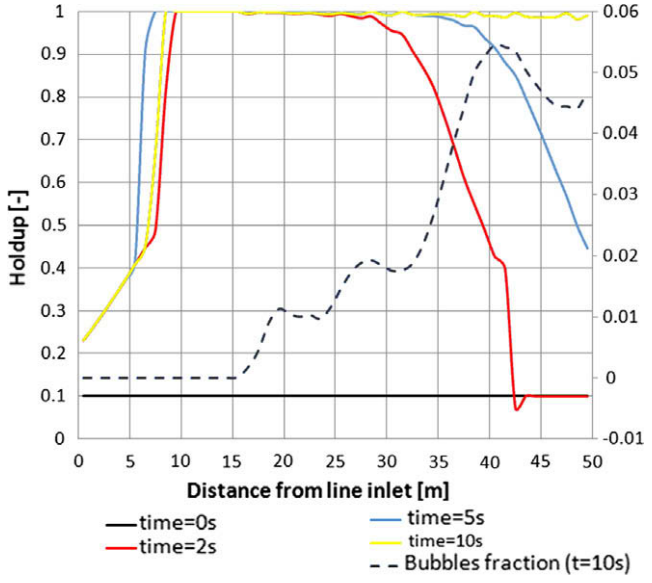

Fig. 11. Liquid layer holdup profiles at different times for bubbly flow case with gas–liquid separated flow fed into the pipe (U_l = 10 m/s, U_g = 1 m/s). the bubble fraction is given as the right ordinate, while the liquid layer fraction (called the holdup) is shown in the left.

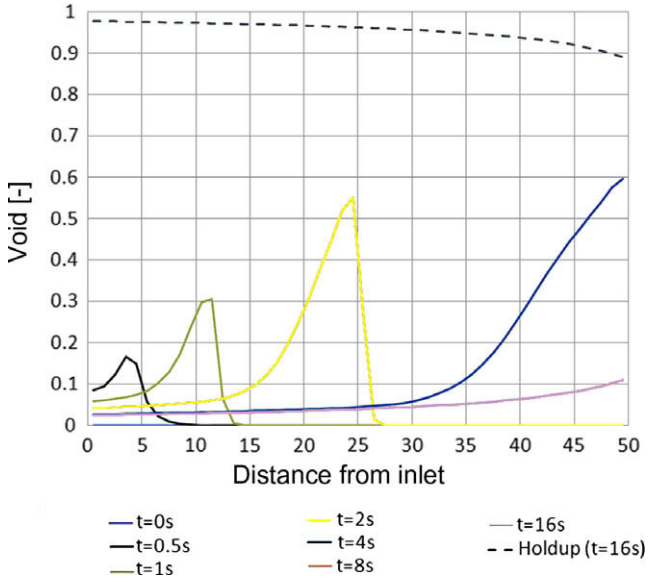

Fig. 12. Propagation of bubbly flow region at different times for bubbly flow case with gas–liquid dispersed flow fed into the pipe (U_m = 11 m/s, ε_b = 0.1). The holdup shown by the dotted line is for the liquid layer, which eventually fills the pipe after 10 s even though the flow was initialized as stratified.

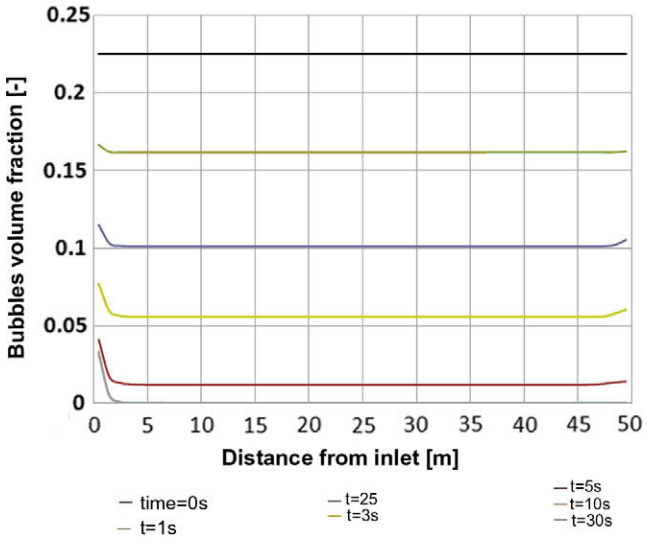

Fig. 13. Bubbles disengagement for dispersed bubbly flow at pipe inlet at low mixture velocity (U_m = 0.1 m/s).

6. Conclusions

An approach based on a four field model, consisting of continuous and dispersed gas and liquid phases has been discussed in the context of providing an innovative flow regime independent formulation for near-horizontal gas–liquid pipeline flows. The model implicitly evolves interfacial area, conforming with the physically-based requirement that the area in dispersed form must be distinguished from the continous area, since the transport processes in each case are very different. Relatively simple flow regime independent closure relationships have been used for the dispersed and continuous phase interactions, as the main point was to determine the validity of the model for first order effects such as flow structure evolution and transitions, which are, to some extent, qualitative in any case. We believe that for the first time, the prediction of several flow regimes has been shown to arise naturally as a part of the calculation, with no special flow regime dependent closure relationships being necessary.

Another finding was that an essential ingredient of the present approach is the adoption of a fine grid, so the calculations converge in a mathematical sense. This requires that, for models of this type, the equation set be hyperbolic, and of course the thatan efficient numerical scheme be developed, which in our case was based on a nearly explicit solution of the model equations to allow for easy parallelization.

It should also be noted that the correct identification of the slug flow pattern discussed in Section 5.2 represents a particularly interesting aspect of the model in that the actual choice of the slug flow identification parameters c_1 and c_2 has a small effect on prediction of transition and on the main slug flow parameters, such as slug velocity and slug length.

The model can only capture phenomena that are dominated by one-dimensional effects and therefore cannot distinguish between annular flow and stratified flow with large interfacial waves, as multidimensional effects may be important in forming the liquid film that wets the whole pipe wall in annular flow. Similarly multidimensional effects can also be expected to be important in churn turbulent flow regimes and would be outside the scope of the proposed model. However, within the scope of these limitations the model does calculate development of the various flow regimes for near-horizontal flows and quantitatively predicts parameters such as slug length and frequency in agreement with data. It is important to note that the solution methods must conserve mass for each of the fields and be capable of achieving the performance needed for high resolution to achieve the results shown here. In future it will be interesting to determine in more detail the effect of different closure relationships and whether a similar approach might be useful for flows in vertical pipelines.

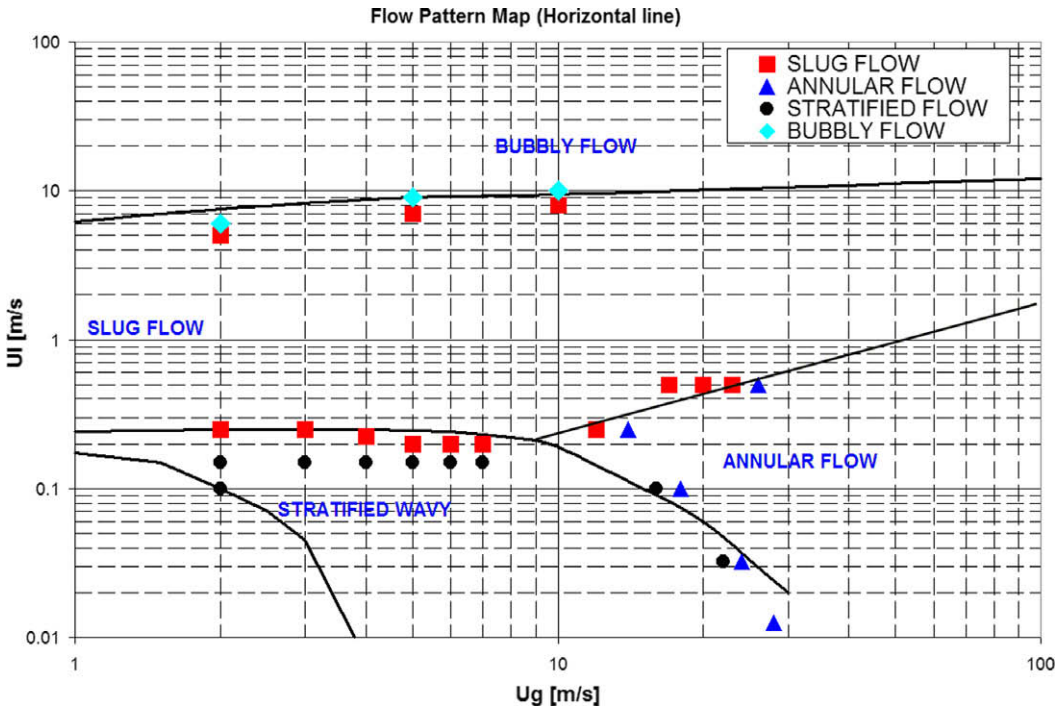

Fig. 14. Comparison between code DPR predictions and mechanistic model of Taitel & Dukler for flow pattern map in a horizontal line.

Acknowledgements

The authors thank ENI for its support through their work. In particular, ENI supported the numerical developments.

Appendix A. Order of magnitude of inertial terms in momentum conservation equation

The left hand sides of the mixture momentum equations for layer 1 and 2 (Eqs. (4) and (5) respectively) can be simplified by looking at the ratio of the momentum fluxes

Rewrite the left hand side of Eq. (4):

$$\frac{\partial(\varepsilon_1\rho_1 u_1)}{\partial t}+\frac{\partial(\varepsilon_1\rho_1 u_1^2)}{\partial z}+\frac{\partial}{\partial z}\left[\left(\frac{\rho_g\rho_l c_b(1-c_b)\varepsilon_1}{\rho_1}\right)u_{s1}^2\right] \tag{A1}$$

Take the ratio of the two momentum fluxes:

$$\text{TERM}=\frac{\rho_1\varepsilon_1 u_1^2}{\frac{\rho_g\rho_l c_b\varepsilon_1(1-c_b)}{\rho_1}u_{s1}^2} \tag{A2}$$

Expanding the terms which are function of the flow variables, equation (A2) can be rewritten as:

$$\frac{\rho_1^2\varepsilon_1}{\rho_g\rho_l c_b(1-c_b)\varepsilon_1}\left(\frac{u_1}{u_{s1}}\right)^2=\frac{\frac{(\varepsilon_l\rho_l+\varepsilon_b\rho_g)^2}{(\varepsilon_l+\varepsilon_b)^2}(\varepsilon_l+\varepsilon_b)}{\rho_g\rho_l\frac{\varepsilon_l\varepsilon_b}{(\varepsilon_l+\varepsilon_b)^2}(\varepsilon_l+\varepsilon_b)}\left(\frac{u_1}{u_{s1}}\right)^2 \tag{A3}$$

Eq. (A3) can be further reduced to:

$$\left[\frac{\varepsilon_l\rho_l}{\varepsilon_b\rho_g}+2+\frac{\varepsilon_b\rho_g}{\varepsilon_l\rho_l}\right]\left(\frac{u_1}{u_{s1}}\right)^2 \tag{A4}$$

Define

$$x=\frac{\varepsilon_l\rho_l}{\varepsilon_b\rho_g} \tag{A5}$$

and Eq. (A4) can then be rewritten as:

$$\left[x+2+\frac{1}{x}\right]\left(\frac{u_1}{u_{s1}}\right)^2 \tag{A6}$$

Differentiate the first member of Eq. (A6) and obtain:

$$F'(x)=1-\frac{1}{x^2} \tag{A7}$$

It is easily shown that the function possesses a minimum when x is equal to 1. Under this occurrence, the term of Eq. (A6) reduces to:

$$\text{TERM}=4\left(\frac{u_1}{u_{s1}}\right)^2 \tag{A8}$$

Since the centre of mass velocity will be typically much higher than the slip velocity, the ratio of the momentum fluxes would then scale as:

$$\text{TERM}\sim O(10)\text{ or greater} \tag{A9}$$

Similarly, for the mixture momentum equation of gas continuous and liquid dispersed (Eq. (5)) the ratio of the momentum fluxes is:

$$\text{TERM}=\frac{\rho_2\varepsilon_2 u_2^2}{\frac{\rho_g\rho_l c_d\varepsilon_2(1-c_d)}{\rho_2}u_{s2}^2} \tag{A10}$$

Following the line of thought outlined for the mixture momentum equation of layer 1, the term can be expanded as follows:

$$\frac{\frac{(\varepsilon_g\rho_g+\varepsilon_d\rho_l)^2}{(\varepsilon_g+\varepsilon_d)^2}(\varepsilon_g+\varepsilon_d)}{\rho_g\rho_l\frac{\varepsilon_g\varepsilon_d}{(\varepsilon_g+\varepsilon_d)^2}(\varepsilon_g+\varepsilon_d)}\left(\frac{u_2}{u_{s2}}\right)^2 \tag{A11}$$

Expanding the terms Eq. (A12) can be reduced to:

$$\left[\frac{\varepsilon_g\rho_g}{\varepsilon_d\rho_l}+2+\frac{\varepsilon_d\rho_l}{\rho_g\varepsilon_g}\right]\left(\frac{u_1}{u_{s2}}\right)^2 \tag{A12}$$

As before, if the following assignment is imposed:

$$x=\frac{\varepsilon_g\rho_g}{\varepsilon_d\rho_l} \tag{A13}$$

Eq. (A12) can then be cast in the following convenient form:

$$\left[x+2+\frac{1}{x}\right]\left(\frac{u_2}{u_{s2}}\right)^2 \tag{A14}$$

Following the approach as detailed for the mixture momentum equation for layer 1, it is easily shown that the momentum flux involving the slip can be neglected also for the mixture momentum equation for layer 2.

References

Alipchenkov, V.M., Nigmatulin, R.I., Soloviev, S.L., Stonik, O.G., Zaichik, L.I., Zeigarnik, Y.A., 2004. A three-fluid model of two-phase dispersed annular flow. Int. J. Heat Mass Transfer 47, 5323–5338.

Andreussi, P., Persen, L.N., 1987. Stratified gas–liquid flow downwardly inclined pipes. Int. J. Multiphase Flow 13, 565–575.

Andreussi, P., Bendiksen, K., Nydal, O.J., 1993a. Void distribution in slug flow. Int. J. Multiphase Flow 19, 817–828.

Andreussi, P., Minervini, A., Paglianti, A., 1993b. A mechanistic model of slug flow in near horizontal pipes. AIChE. J. 39, 1281–1291.

Andreussi, P., Paglianti, A., Sanchez, F., 1999. Dispersed bubble flow in horizontal pipes. Chem. Eng. Sci. 54, 1101–1107.

Andritsos, N., Hanratty, T.J., 1987. Influence of interfacial waves in stratified gas–liquid flows. J. AIChE. 33, 444–454.

Andritsos, N., Williams, L., Hanratty, T.J., 1989. Effect of liquid viscosity on the stratified-slug transition in horizontal pipe flow. Int. J. Multiphase Flow 15, 877–892.

Banerjee, S., Chan, A.M.C., 1980. Separated flow models 1. Analysis of the averaged and local instantaneous formulations. Int. J. Multiphase Flow 6, 1–24.

Barnea, D., Taitel, Y., 1993. Kelvin–Helmholtz stability criteria for stratified flow: Viscous versus non-viscous (inviscid) approaches. Int. J. Multiphase Flow 19, 639–649.

Barnea, D., Taitel, Y., 1994. Non-linear interfacial instability of separated flow. Chem. Eng. Sci 49, 2341–2349.

Bendiksen, K., 1984. Experimental investigation of the motion of long bubbles in inclined tubes. Int. J. Multiphase Flow 10, 467–483.

Bendiksen, K., Malnes, D., Moe, R., Nuland, S. 1991. The dynamic two-fluid model OLGA: Theory and Application. SPE Paper 19451, 171–180.

Cohen, L.S., Hanratty, T.J., 1968. Effect of waves at a gas–liquid interface on a turbulent air flow. J. Fluids Mech. 31, 467.

Delhaye, J.M., Achard, J.L. 1977. On the averaging operators introduced in two-phase flow modeling. Thermal and Hydraulic Aspects of Nuclear Reactor Safety. Light Water Reactors, ASMEE Winter Meeting.

Dukler, A.E., Hubbard, M.G., 1975. A model for gas–liquid slug flow in horizontal and near horizontal tubes. I& EC Fundam. 14, 337–347.

Ferziger, J.H., Peric, M., 1999. Computational methods for fluid dynamics. Springer, Germany.

Hall, N.A., 1957. Thermodynamics of fluid flow. Longmans, Green and Co.

Hall, D.G., Johnson, E.C., 1982. RELAP5/MOD1 Quick Reference Manual. EGG-CDD-6027.

Harlow, F.H., Welch, J.E., 1965. Numerical calculation of time-dependent viscous incompressible flow of fluid with free surface. Phys. Fluids 8, 2182–2189.

Holmas, H., Sira, T., Nordsveen, M., Lantiangen, H.P., Schulkes, R., 2008. Analysis of a 1D incompressible two-fluid model including artificial diffusion. IMA J. Appl. Math.

Hurlburt, E.T., Hanratty, T.J., 2002. Prediction of the transition from stratified to slug and plug flow for long pipes. Int. J. Multiphase Flow 28, 707–729.

Ishii, M., 1975. Thermo-fluid dynamic theory of two-phase flows. Eyrolles, Paris.

Kadri, U., Mudde, R.F., Oliemans, R.V.A. 2007. On the prediction of the transition from stratified flow to roll waves and slug flow in horizontal pipes. In: 13th Int. Conf. Multiphase Production Technology, Edinburgh, UK 13–15 June.

Kawaji, M., Banerjee, S., 1987. Application of a two-field model to reflooding of a hot vertical tube-i. model structure and interfacial phenomena. J. Heat Transfer 109, 204–211.

Lin, P.Y., Hanratty, T.J., 1986. Prediction of the initiation of slugs with linear stability theory. Int. J. Multiphase Flow 12, 79–98.

Lioumbas, J.S., Paras, S.V., Karabelas, A.J., 2005. Co-current stratified gas–liquid downflow – Influence of the liquid flow field on interfacial structure. Int. J. Multiphase Flow 31, 869–896.

Louaked, M., Hanich, L., Thompson, C.P., 2003. Well-posedness of incompressible models of two- and three-phase flow. IMA J. Appl. Math. 68, 595–620.

Micaelli, J.C. 1987 CATHARE An advanced best-estimate code for PWR safety analysis. SETh/LEML-EM/87-58.
Nydal, O.J., Andreussi, P., 1991. Gas entrainment in a long liquid slug advancing in a near horizontal pipe. Int. J. Multiphase Flow 17, 179–189.
Nydal, O.J., Pintus, S., Andreussi, P., 1992. Statistical characterization of slug flow in horizontal pipes. Int. J. Multiphase Flow 18, 439–453.
Nydal, O.J., Banerjee, S., 1996. Dynamic slug tracking simulations for gas–liquid flow in pipelines. Chem. Eng. Comm. 141–142, 13–39.
Pan, L., Hanratty, T.J., 2002. Correlation of entrainment for annular flow in horizontal pipes. Int. J. Multiphase Flow 28, 385–408.
Pauchon, C., Dhulesia, H., Binh-Cirlot, G., Fabre, J. 1994. TACITE: A transient tool for multiphase pipeline and well simulation. SPE Annu. Tech. Conf. And Exhibition, SPE Paper 28545, New Orleans, LA, US.
Sarkhi, A.Al., Hanratty, T.J., 2002. Effect of pipe diameter on the drop size in a horizontal annular gas–liquid flow. Int. J. Multiphase Flow 28, 1617–1629.
Spedding, P.L., Hand, N.P., 1997. Prediction in stratified gas–liquid co-current flow in horizontal pipelines. Int. J. Heat Mass Transfer 40, 1923–1935.
Taitel, Y., Dukler, A.E., 1976. A model for predicting flow regime transitions in horizontal and nearly horizontal gas–liquid flow. J. AIChE 22, 47–55.
Tomiyama, A., Kataoka, I., Fukuda, T., Sakaguchi, T., 1995. Drag coefficient of bubbles (2^{nd} report, drag coefficient for a swarm of bubbles and its applicability to transient flow). Trans. Japan Soc. Mech. Eng. B, 46–53.
Wallis, G.B., 1969. One-dimensional two-phase flow. McGraw-Hill.
Vernier, P., Delhaye, J., 1968. General two-phase flow equations applied to the thermodynamics of boiling nuclear reactors. Energ. Primarie 4, 1–43.